THE JOURNAL OF PHYSICAL CHEMISTRY A

Article

Cite This: J. Phys. Chem. A 2018, 122, 9403−9411

pubs.acs.org/JPCA

# NEXMD Modeling of Photoisomerization Dynamics of 4-Styrylquinoline

Andrew E. Sifain,[†,‡] Brendan J. Gifford,[‡] David W. Gao,[¶,‡] Levi Lystrom,[§,‡] Tammie R. Nelson,[‡] and Sergei Tretiak*[,∥,‡]

[†]Department of Physics and Astronomy, University of Southern California, Los Angeles, California 90089-0485, United States

[‡]Theoretical Division and Center for Nonlinear Studies, Los Alamos National Laboratory, Los Alamos, New Mexico 87545, United States

[¶]Los Alamos High School, Los Alamos, New Mexico 87544, United States

[§]Department of Chemistry and Biochemistry, North Dakota State University, Fargo, North Dakota 58108, United States

[∥]Center for Integrated Nanotechnologies, Los Alamos National Laboratory, Los Alamos, New Mexico 87545, United States

Supporting Information

**ABSTRACT:** Isomerization of molecular systems is ubiquitous in chemistry and biology, and is also important for many applications. Atomistic simulations can help determine the tunable parameters influencing this process. In this paper, we use the Nonadiabatic EXcited state Molecular Dynamics (NEXMD) software to study the photoisomerization of a representative molecule, 4-styrylquinoline (SQ). *trans*-SQ transforms into dihydrobenzophenanthridine (DHBP) upon irradiation with laser light, with the *cis* conformer acting as an intermediate. We study how varying three different external stimuli (i.e., apolar versus polar solvent, low versus high photoexcitation energy, and vacuum versus a constant temperature thermostat) affects the *trans*-to-*cis* photoisomerization of SQ. Our results show that polarization effects due to implicit solvation and the thermostat play a crucial role in the isomerization process, whereas photoexcitation energy plays a lesser role on the outcome and efficiency. We also show that NEXMD captures the correct energy profile between the ground and first singlet excited state, showing that there are two distinct reaction pathways to the final stable product that vary by the number of photons absorbed, in agreement with experiment. Ultimately, NEXMD proves to be an effective tool for investigating excited state single molecule dynamics subject to various environments and initial conditions.

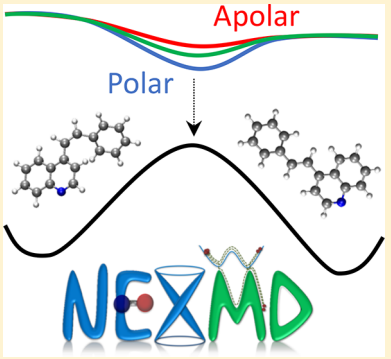


## 1. INTRODUCTION

On a molecular scale, optical energy can be converted into mechanical and chemical energy through isomerization.[1] In many organic molecules, this conversion manifests itself through the *trans*-to-*cis* or *cis*-to-*trans* conformational change around C=C bonds[2] and involves pathways mediated by conical intersections.[3] Studying this process is key to understanding many common yet complex processes including vision,[4,5] ion pumping,[6] and organic synthesis.[7] Photoisomerization is also important for technological applications such as biomimetic materials,[8,9] conductive polymers,[10] and optical data storage.[11−13]

Computational modeling of isomerization in organic molecules not only reveals how this process occurs in nature but also helps identify ways of controlling the dynamics via external stimuli.[14] One such example is solvation, as it has shown to influence isomerization both in terms of time scales and reaction pathways.[15−23] Molecular dynamics simulations can be used to determine the effects of solvation by capturing the changes in molecular geometry and potential energy surfaces (PESs) involved in the reaction.[24] Other external factors (or tunable stimuli) that can influence isomerization include photoexcitation energy[20,25] and the thermostat.[26] In this paper, we study the effects of these three external stimuli on the *trans*-to-*cis* photoisomerization of 4-styrylquinoline using the Nonadiabatic EXcited state Molecular Dynamics (NEXMD) software.

4-styrylquinoline is an organic conjugated molecule that isomerizes upon irradiation with laser light.[27] Compared to other commonly studied molecules that undergo isomerization, such as azobenzenes,[28−32] stilbenes,[32−36] and ethylenes,[1,16,36,37] 4-styrylquinoline is slightly larger in size; it might be a difficult task for a first-principles level of theory to compute the excited state dynamics due to the computational costs. Such numerically prohibitive theories include grid-based methods or multiconfigurational time-dependent Hartree−Fock.[1] Instead, we run our simulations with NEXMD, which uses numerically efficient semiempirical Hamiltonian models, and a swarm of classical nuclear trajectories that undergo nonadiabatic transitions between excited states via surface

**Received:** September 17, 2018
**Revised:** November 1, 2018
**Published:** November 2, 2018







DOI: 10.1021/acs.jpca.8b09103
J. Phys. Chem. A 2018, 122, 9403−9411

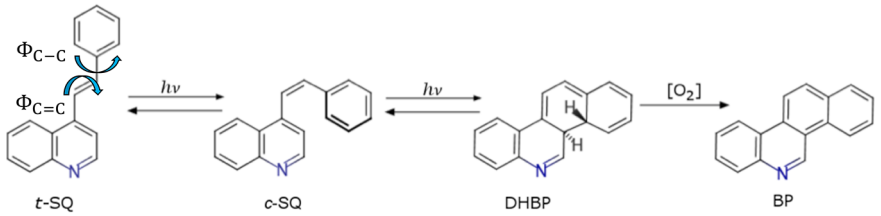


**Figure 1.** Photoexcitation of *t*-SQ results in a transformation to DHBP, with *c*-SQ being an intermediate in the reaction. Once DHBP is formed, it is then possible to undergo a final transformation from DHBP to BP with the addition of oxygen.

hopping.[38−48] But the more compelling reason to study 4-styrylquinoline is its unique isomerization process, as it has been experimentally shown to proceed from its *trans* conformation to its final stable product along one of two different reactions pathways that vary by the number of photons absorbed. Studying 4-styrylquinoline thus poses the opportunity to complement experimental findings, provide a detailed investigation of some of the external factors influencing its photoisomerization, and benchmark the capabilities of NEXMD against a relatively difficult molecule to model from first principles.

## 2. COMPUTATIONAL DETAILS

**2.1. Ground State Sampling.** The ground state geometries of *t*-SQ, *c*-SQ, DHBP, and BP were optimized with the AM1 semiempirical Hamiltonian.[49] Born−Oppenheimer molecular dynamics were then performed on the ground state using AM1. An implicit linear response solvent model was coupled to the dynamics to simulate the electrostatic effects of solvation.[50] The induced polarization due to Coulombic interactions at the solute−solvent boundary increases with the dielectric constant of the solvent $\epsilon$ and obeys $f(\epsilon) = (\epsilon - 1)/\epsilon$. The interaction at the solute−solvent boundary produces an electrostatic potential, which is added to the solute's Hamiltonian. The additional effect of the induced polarization progressively decreases as $\epsilon$ increases since $f(\epsilon)$ asymptotically approaches one.[48,51] We limit ourselves to two solvents with low and high polarity—an apolar solvent of *n*-hexane ($\epsilon \approx 2$) and a polar solvent of ethanol ($\epsilon \approx 25$). These two solvents were also used in the associated experimental work.[27] Two separate ground state trajectories for each species that are shown in Figure 1 were simulated, differing only in solvent environment. Ground state trajectories were 1 ns in length with a 0.5 fs time step. Nuclear dynamics were described by the Langevin equation at a temperature set to 300 K and friction parameter of 20 $ps^{-1}$.[48] Snapshots (i.e., coordinates and velocities) of each species were recorded throughout these trajectories and were used as initial conditions for all subsequent NEXMD simulations of the excited states.

**2.2. Optical Absorption Spectra.** Singlepoint calculations were performed at the ground state geometries to determine vertical excitation energies and oscillator strengths. Excited states were calculated using the collective electronic oscillator (CEO) method combined with AM1.[52,53] Implicit solvation was also included in singlepoint calculations. About 10 excited states were required to model absorption up to 200 nm. Oscillator strengths were Gaussian-broadened at the excitation energies with an empirical standard deviation of 0.15 eV. For each environment, an average over all absorption spectra, one for each snapshot, formed the convoluted theoretical absorption spectrum (Figure 2).

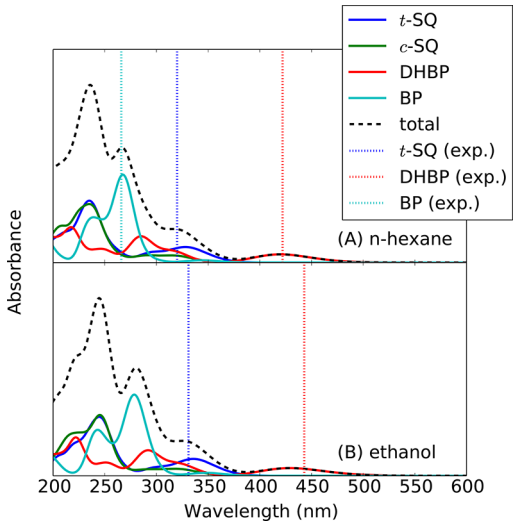


**Figure 2.** Optical absorption spectra of *t*-SQ, *c*-SQ, DHBP, and BP in (A) *n*-hexane and (B) ethanol. Wavelengths of peak maxima from experimental absorption bands are shown with dashed vertical lines. Theoretical spectra were blueshifted by 0.45 eV.

**2.3. Photoexcitation to $S_1$: Adiabatic Dynamics.** The photoisomerization process involves the conical intersection between the first singlet excited state ($S_1$) and the ground state ($S_0$). Therefore, we begin our analysis by performing adiabatic dynamics on $S_1$ in each solvent environment. Following vertical excitation to $S_1$, trajectories were propagated for a maximum of 50 ps with a classical time step of 0.50 fs using the same Langevin thermostat as the ground state trajectories. A cartoon schematic of this low-energy (i.e., $S_0 \rightarrow S_1$) simulation is shown in Figure 3.

**2.4. Analysis of NEXMD of Geometries.** In order to determine the reaction pathways, we analyzed the geometries along the adiabatic NEXMD trajectories described in the section 2.3. We combined the geometries of several dynamical simulations that were initialized with *t*-SQ and *c*-SQ ground state geometries. Geometries sampled from adiabatic trajectories on $S_1$ were analyzed with a Ramachandran diagram[54] of $\phi_{C=C}$ and $\phi_{C-C}$ (Figure 4A). Changes in the potential energy manifests itself in rotation about these two dihedral angles. $S_1$ adiabatic dynamics trajectories starting from *t*-SQ geometries were used to sample geometries with $\phi_{C=C} > 90°$. The conical intersection of *p*-SQ, located at $\phi_{C=C} \approx 90°$ (Figure 3), was approached but not passed through (i.e., $\phi_{C=C} < 90°$). Another set of simulations starting from *c*-SQ provided sampled initial geometries with $\phi_{C=C} < 90°$, including DHBP. Rotational symmetry around both $\phi_{C-C}$ and $\phi_{C=C}$ results in chemically similar structures. For $\phi_{C-C}$, a $C_2$ symmetry axis makes the following angles equivalent: $\phi_{C-C} = -180°$, 0°, and 180°. Likewise, structures with $\phi_{C=C} = -90°$ and +90° are also


DOI: 10.1021/acs.jpca.8b09103
J. Phys. Chem. A 2018, 122, 9403−9411

chemically similar. Figure 4B labels the different conformers on the Ramachandran diagram (Figure 5).

Molecular orbitals (MOs) were used to describe chemical effects that dictate the reaction pathways. Since geometries of interest are those that are generated along trajectories from *t*-SQ to DHBP, passing through both *p*-SQ and *c*-SQ, a continuous scan was performed by changing $\phi_{C=C}$ from 180° (*t*-SQ) to 0° (*c*-SQ). This procedure generated the potential energy surface (PES) of isomerization, and was accomplished by continuously varying the distance between two chosen carbon atoms of SQ (Figure 4A). When the interatomic distance between these two atoms is large, the only plausible conformation is *t*-SQ. As interatomic distance decreases, *p*-SQ, *c*-SQ, and DHBP become favorable.

**2.5. Isomerization Rate.** Nonadiabatic transitions to $S_0$ are not explicitly simulated in NEXMD as a result of the inability to describe crossings between a multireference excited state (CIS) and a single-reference ground state (Hartree−Fock).[55] Instead, we apply a simple model based on energy gaps to qualitatively describe $S_1 \rightarrow S_0$ transitions. Since nonadiabatic coupling scales inversely with energy gap, transitions are very likely to occur at geometries near *p*-SQ (located near $\phi_{C=C} \approx 90°$ of Figure 6). In general, however, trajectories can transition at finite energy gaps before reaching the conical intersection. We set a $\Delta E$ = 1.0 eV (Figure 3) threshold on the energy gap to qualitatively describe the rate at which trajectories approach the conical intersection and subsequently transition to $S_0$.[66] A similar procedure has been applied in works pertaining to photodissociation dynamics.[56] Figure 7 shows the fraction of trajectories with at least one occurrence where the energy gap fell below 1.0 eV and thus can be interpreted as the fraction of trajectories that have reached the conical intersection.

**2.6. High-Energy Photoexcitation: Nonadiabatic Dynamics.** In order to understand the effect of excitation energy on isomerization, we perform nonadiabatic dynamics from an initial high-energy state, $S_n$ ($n > 1$). The excess electronic energy must first be converted to vibrations during the $S_n \rightarrow S_1$ internal conversion process. On the basis of the absorption spectra of Figure 2, the laser excitation energy was chosen to excite the bright peak at approximately 260 nm. Nonadiabatic dynamics used the same 500 snapshots from *t*-SQ ground state trajectories as those used for adiabatic dynamics on $S_1$. The initial excited state, $S_n$, was chosen according to the absorption spectrum of the corresponding molecular structure, such that excited states with larger oscillator strengths were more populated than those with lower oscillator strengths. This procedure models a photoexcited wave packet sampling the phase space of different nuclear configurations at room temperature. We find that $S_6$ is the most populated state, but due to thermal fluctuations, states in close vicinity to $S_6$ are also populated due to diabatic state crossings. Trajectories were propagated for 1 ps, with a classical time step of 0.10 fs (nuclei) and quantum time step of 0.02 fs (electrons), using the same Langevin thermostat as the ground state trajectories. Nonadiabatic transitions between excited states were modeled with Tully's fewest switches surface hopping.[57] Electronic decoherence[58] and transitions at unavoided (trivial) crossings[59] were treated with established methods within the NEXMD framework. A cartoon schematic of this high-energy simulation (labeled "nonadiabatic dynamics") is shown in Figure 3.

**2.7. Constant Energy Dynamics.** In order to assess the effect of the thermostat on nonradiative relaxation from $S_m$ to $S_1$ and subsequent isomerization, we performed the same aforementioned nonadiabatic simulations from the initial high-energy $S_m$ state with the thermostat turned off, corresponding to constant energy Newtonian dynamics. For these simulations, we used the same ground state sampling as preceding simulations, thus making it feasible to isolate the effects of the bath. For both low- and high-energy simulations (Figure 3), the solvent model was turned off (i.e., $\epsilon = 1$). Upon photoexcitation, it is expected that optical energy will be converted into nuclear vibrational energy. In a simulation with nuclei coupled to the Langevin equation, a portion of the vibrational energy is dissipated to the bath. Since the dissipation is absent in Newtonian simulations, the effect of the bath on the isomerization can be determined.

## 3. RESULTS AND DISCUSSION

The following section is organized as follows. First, we provide an overview of the conformations of SQ during isomerization (Figure 1). We then compute the optical absorption spectra and compare the theoretical results to the experimental absorption maxima (Figure 2). Finally, we present results of the dynamical simulations in the presence of different environments. These simulations are carried out at both low and high photoexcitation energies, corresponding to adiabatic and nonadiabatic dynamics, respectively (Figure 3). As part of our discussion, we describe the reaction pathways by analyzing SQ conformations and the potential energy surfaces (PESs) involved in the isomerization process (Figure 5). We also measure the isomerization rate, mediated by transitions through the conical intersection between the first singlet excited state ($S_1$) and the ground state ($S_0$) (Figure 7 and Table 1). For the high-energy (nonadiabatic) simulations, we compute nonradiative relaxation rates and show that electronic relaxation to $S_1$ is primarily coupled to carbon−carbon stretching modes (Figure 8). Computational details of all simulations are provided in section 2.

**3.1. 4-Styrylquinoline (SQ).** The experimental work of ref 27 has described the conformations of SQ during isomerization. The reaction from the *trans* conformer (*t*-SQ) to its final stable product is shown in Figure 1. *t*-SQ is the most stable in the ground state because of lack of steric hindrance between the quinoline and phenyl rings. When the central double bond between the rings (labeled $\phi_{C=C}$) is rotated by 90°, the quinoline and phenyl rings are in a nonplanar orientation. This structure is denoted as the *perp* conformer (*p*-SQ) (not shown in Figure 1, but will be discussed further). Rotating $\phi_{C=C}$ by another 90° generates the *cis* conformer (*c*-SQ). This process is met with significant destabilization due to steric hindrance between the quinoline and phenyl rings. Simultaneous rotation of the C−C bond adjacent to C═C and the phenyl ring (labeled $\phi_{C-C}$) increases the distance between hydrogen atoms on the rings, which alleviates torsional strain and results in a structure with nearly perpendicular quinoline and phenyl rings. Rotation about $\phi_{C-C}$, such that both rings are nearly coplanar, can only be accomplished with a change in hybridization of one carbon atom in each ring, thus forming dihydrobenzophenanthridine (DHBP). DHBP becomes benzophenanthridine (BP) with the addition of oxygen.

**3.2. Optical Absorption Spectra.** Optical absorption spectra of the different species, calculated in both *n*-hexane and ethanol, are shown in Figure 2. The line shape labeled by *total*



DOI: 10.1021/acs.jpca.8b09103
J. Phys. Chem. A 2018, 122, 9403−9411

is the sum of all species, which we directly compare to the experimental absorption maxima of ref 27., shown as dashed lines in Figure 2. Each absorption peak of ref 27 is assigned to a different species. The peaks of interest are the three low-energy peaks, spanning the range of 500−250 nm. The low- and high-energy peaks are assigned to DHBP and BP, respectively. On the basis of the theoretical results of Figure 2, these assignments are in excellent agreement. The peak between 350−300 nm is experimentally assigned to *t*-SQ. Although *t*-SQ theoretically absorbs within this range, Figure 2 shows that *c*-SQ and DHBP may also contribute to the absorption; reduction of the 350−300 nm peak may not be from the decay of *t*-SQ alone, thus making it difficult to determine the *trans*-to-*cis* isomerization rate from an experimental perspective.

In order to support the use of the semiempirical level of theory carried out with NEXMD, theoretical and experimental absorption spectra are compared to each other. The *total* spectrum was uniformly blueshifted, such that the low-energy peak of DHBP matched the experimental value at 422 nm. By doing so, the high-energy peak of BP was shifted to about 267 nm. The experimental wavelength of the corresponding DHBP peak is reported to be 266 nm. Errors ranging between 0.10−0.20 eV are seen in the peaks assigned to *t*-SQ in both *n*-hexane and ethanol. The ethanol spectra are red-shifted relative to those in *n*-hexane, which is expected due to stabilization in polar environments. The main theoretical DHBP peak is red-shifted from about 422 to 429 nm (≈ 0.05 eV redshift), while experimentally measured maxima are 422 and 443 nm (≈0.14 eV redshift), respectively. Despite consistent shifts in the data between theory and experiment, the semiempirical level of theory used in the present study appears to provide an accurate description of excited states. A further comparison of the absorption spectra using density functional theory (DFT) is presented in the Supporting Information (Figures S1 and S2).

**3.3. Photoisomerization Reaction Pathway.** The reaction pathway for the photoisomerization process was determined from the geometries collected from NEXMD trajectories. A schematic of the dynamical simulations that were initialized with low and high photoexcitation energies is shown in Figure 3. In the current subsection, we describe the isomerization pathways in terms of the low-energy simulation since the process itself occurs between $S_1$ and $S_0$. For this analysis, conformations of SQ are labeled by the two dihedral angles, $\phi_{C-C}$ and $\phi_{C=C}$, as they are the degrees of freedom that predominantly dictate the potential energy of the system (Figure 4A). Figure 4B represents the different conformers in terms of a phase diagram, which is more formally known as a Ramachandran diagram.[54]

Figure 5 shows the Ramachandran diagram that was made using geometries from dynamical simulations on $S_1$. Geometries were compared to those generated by the PES scan (Supporting Information, Figure S3). General agreement between the structures allows us to use scanned geometries for MOs. The predominant transition contributing to the $S_1$ excitation is $\pi \rightarrow \pi^*$ between the highest-occupied molecular orbital (HOMO) and lowest-unoccupied molecular orbital (LUMO). These MOs are used to describe the reaction of Figure 1 with regards to excitation and relaxation during isomerization and subsequent formation of DHBP (Supporting Information, Figure S4).

The following discussion is in reference to Figure 5 and the MOs presented in the Supporting Information (Figure S4). *t*-

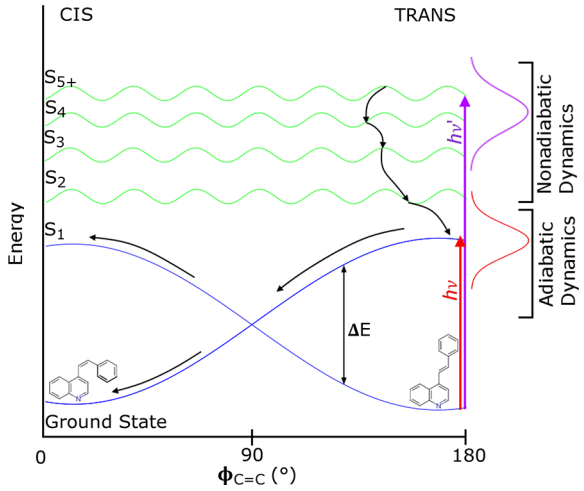


**Figure 3.** Cartoon schematic of NEXMD simulations of the SQ molecule. Simulations were performed at low ($h\nu$) and high ($h\nu'$) photoexcitation energies beginning with *t*-SQ in the ground state. The schematic only shows *t*-SQ → *c*-SQ. The low- and high-energy simulations are modeled as adiabatic and nonadiabatic dynamics, respectively. While both processes are nonadiabatic in practice, NEXMD cannot explicitly simulate nonadiabatic transitions between $S_1$ and $S_0$. As a result, dynamics always end on $S_1$. Further computational details of the NEXMD theory as well as the approach taken to qualitatively model $S_1 \rightarrow S_0$ transitions are available in section 2.

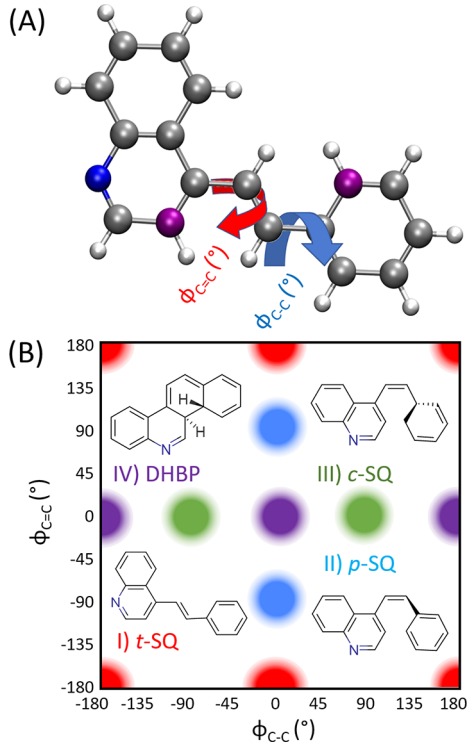


**Figure 4.** (A) Labeling of $\phi_{C=C}$ and $\phi_{C-C}$ dihedral angles. The two carbons atoms colored in purple were used for the PES scan. (B) Different conformations of SQ during isomerization that are identified by the dihedrals.

SQ minimizes steric hindrance and is a local minimum in the ground state. Photoexcitation of *t*-SQ (**I**) creates an unstable nodal structure in the orbital, resulting in a local energy gap maximum. This nodal structure places strain on the C═C


DOI: 10.1021/acs.jpca.8b09103
J. Phys. Chem. A 2018, 122, 9403−9411

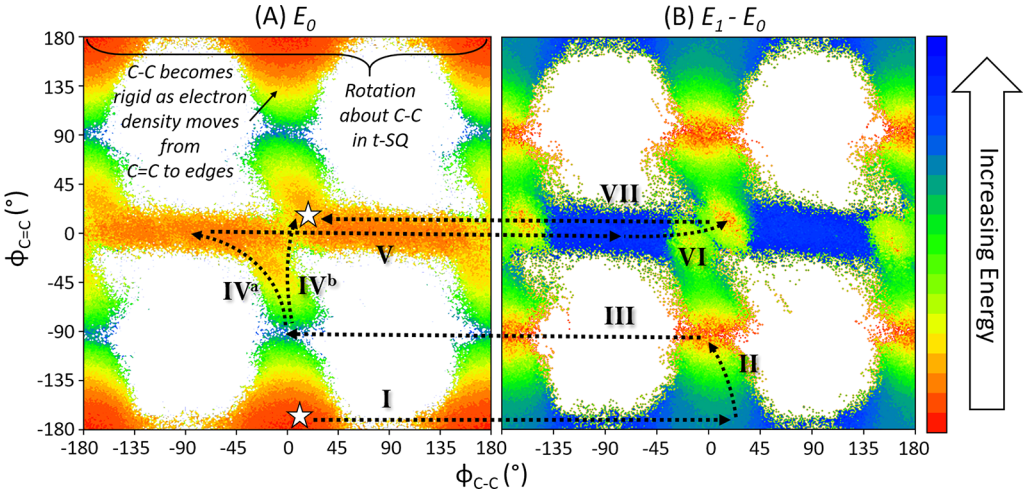


**Figure 5.** Ramachandran diagram of the low-energy excitation to $S_1$ in apolar solvent. (A) shows relative energy of the ground state $S_0$ and (B) shows the relative energy of the gap $E_1 - E_0$. Arrows are included to show photoexcitation, nonradiative relaxation, and movement along the PESs. **I**: $S_0 \rightarrow S_1$ photoexcitation at *t*-SQ. **II**: *t*-SQ → *p*-SQ in $S_1$. **III**: $S_1 \rightarrow S_0$ nonadiabatic transition at *p*-SQ. **IV**$^a$: *p*-SQ → *c*-SQ in $S_0$. **IV**$^b$: *p*-SQ → DHBP in $S_0$. **V**: $S_0 \rightarrow S_1$ photoexcitation at *c*-SQ. **VI**: *c*-SQ → DHBP in $S_1$. **VII**: $S_1 \rightarrow S_0$ nonadiabatic transition at DHBP.

bond, which is alleviated with a change in $\phi_{C=C}$. The molecule twists from *t*-SQ to *p*-SQ (**II**). This process reduces $\pi-\pi$ overlap in the C═C bond, which shifts electron density from the central bond to the adjacent phenyl ring.[60] For *p*-SQ, the HOMO is localized on the quinoline ring while the LUMO is localized on the phenyl ring. After $\phi_{C=C}$ reaches 90°, the molecule transitions to the ground state through the conical intersection (**III**), and electron density simultaneously moves back to the quinoline ring. The ground state no longer has a node in the central C═C bond. At this point, there are two distinct pathways that are energetically accessible. The molecule may twist toward *c*-SQ (**IV**$^a$) or directly form DHBP (**IV**$^b$). For the former, the steric hindrance between the quinoline and phenyl rings requires $\phi_{C-C}$ to rotate 90°. A simultaneous rotation of $\phi_{C=C}$ generates *c*-SQ. The second pathway is a direct formation of DHBP through a 90° rotation of $\phi_{C=C}$. Hence, the second pathway is a one photon process.

In the case of **IV**$^a$, *c*-SQ is a local minimum on the ground state, and therefore another excitation is required to undergo a transition to DHBP (**V**). In the excited state, *c*-SQ is a local maximum and DHBP is a local minimum; formation of a bond connecting the quinoline and phenyl rings creates DHBP (**VI**). The two carbon atoms of the newly formed bond change hybridization from $sp^2$ to $sp^3$ character. The final DHBP product is stable following subsequent relaxation back to the ground state (**VII**). The driving force of the reaction and fundamental conformations are well replicated using NEXMD. The energy profile of the reaction suggests that there are two pathways from *t*-SQ to DHBP that differ by the number of photons absorbed (Figure 1).

**3.4. *Trans*-to-*Cis* Photoisomerization Dynamics.** Adiabatic dynamics on the $S_1$ PES were initialized with *t*-SQ geometries. Figure 6A shows energies of the ground ($E_0$) and first excited state ($E_1$) as a function of $\phi_{C=C}$ taken from every geometry and at every time step along all trajectories of the ensemble. The energy gaps $E_1 - E_0$ were also plotted as a function of $\phi_{C=C}$ (Figure 6B). The positive correlation between the energy gap and $\phi_{C=C}$ shows the progression of the molecule toward *p*-SQ as the energy gap decreases. Increasing solvent polarity both stabilizes the energy levels (Figure 6A) and decreases the energy gaps in more polar solvents (Figure 6B); $E_0$ decreases by approximately 0.25 eV from $\epsilon$ = 1 to ethanol while $E_1$ decreases by approximately 0.50 eV. A significant change in the energy gap affects nonadiabatic transitions, $S_1 \rightarrow S_0$, thus influencing the isomerization rate.

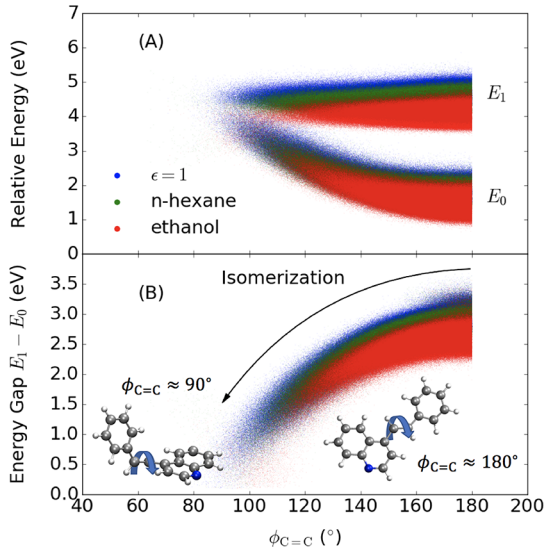


**Figure 6.** (A) Energies of the ground ($E_0$) and first excited state ($E_1$) as a function of $\phi_{C=C}$. (B) Energy gap $E_1 - E_0$ as a function of $\phi_{C=C}$.

The plots of Figure 7 show the trajectory ensemble reaching the conical intersection and provide a time scale for the *trans*-to-*cis* conversion. Table 1 shows time scales $\tau$ of *trans*-to-*cis* from the following stimuli: solvation, photoexcitation energy, and constant temperature thermostat. Isomerization rate increases with solvent polarity; the relaxation rate is approximately twice as fast in the polar solvent than the apolar solvent. In ref27., the magnitude of the *t*-SQ absorption peak decreases in time, thus showing the decay of *t*-SQ. *t*-SQ decays faster in ethanol than *n*-hexane, in agreement with calculations. It is also interesting that the ratio of the relaxation time scales are in agreement, i.e., $\tau_{n-hexane}/\tau_{ethanol} \approx 2.1$ (theory) and ≈1.6 (experiment) (see further discussion in Supporting Information, Figure S5). With regard to photoexcitation energy, we find that it does not affect isomerization


DOI: 10.1021/acs.jpca.8b09103
J. Phys. Chem. A 2018, 122, 9403−9411

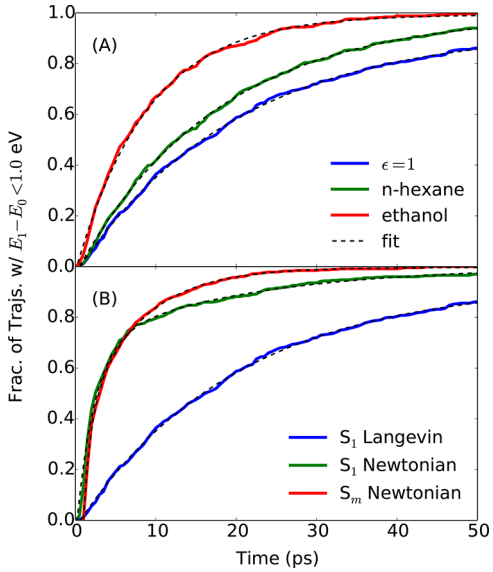


**Figure 7.** Fraction of trajectories evolving on $S_1$ that encountered an energy gap $E_1 - E_0 < 1.0$ eV. (A) Simulations were performed in a Langevin thermostat. (B) Same as part (A) but performed with $\epsilon = 1$.

**Table 1. Time Evolution Associated with the Fraction of Trajectories Evolving on $S_1$ That Encountered an Energy Gap $E_1 - E_0 < 1.0$ eV[a]**

| photoexcitation energy | *n*-hexane | ethanol | $\epsilon = 1$ (Langevin) | $\epsilon = 1$ (Newtonian) |
|---|---|---|---|---|
| low energy: $S_1$ | 18.8 | 8.97 | 19.9 | 2.26, 20.2 |
| high energy: $S_m$ (4.5 eV) | 16.4 | 8.90 | 20.7 | 0.991, 6.91 |

[a]Nuclei evolve according to Langevin (at 300 K) or energy-conserving Newtonian dynamics. Langevin dynamics data were fit to $A - B \exp(-t/\tau)$. Newtonian dynamics were only computed with $\epsilon = 1$, and the data were fit to a double exponential function of the form $A - B \exp(-t/\tau_1) - C \exp(-t/\tau_2)$, where $\tau_1$ and $\tau_2$ are fast and slow time scales, respectively. Time scales shown are in ps.

rate in different solvents, assuming nuclei are coupled to a thermostat. Isomerization rate does however depend on photoexcitation energy if nuclear dynamics evolve in vacuum as opposed to a thermostat. However, this dependence is not so surprising since dynamics in vacuum are energy conserving and therefore excess photoexcitation energy (i.e., $S_m$–$S_1$) will be transferred to nuclear kinetic energy.

For simulations in vacuum with the thermostat absent (Figure 7B, Newtonian), the isomerization rate took the form of a double exponential function with fast and slow time scales. We partition the trajectories into two sets, one for each rate, according to a threshold, which was chosen based on the exponential fit. We find that the difference in isomerization rate is related to energy redistribution of the molecule, where the total amount of initial energy present is dependent on the potential energy of the starting configurations. For trajectories that start with $\phi_{C-C} \sim 90°$, potential energy is the highest, while those with $\phi_{C-C} \sim 0°$, potential energy is the lowest. The $\pi$-orbitals on the C–C bond are the same phase in *t*-SQ; rotation about this bond destabilizes the structure. Ramachandran diagrams of each set of trajectories shows the distribution of $\phi_{C-C}$ being narrower for the slow trajectories than the fast trajectories (Supporting Information, Figures S6 and S7). Trajectories that begin in an unstable conformation transfer energy between potential and kinetic. Rapid motion of the molecule around $\phi_{C-C}$ due to this *excess* energy eventually leads to a faster transformation from *t*-SQ to *p*-SQ through a rotation around $\phi_{C=C}$. The distribution of $\phi_{C-C}$ for a large number of conformations in the slow trajectories remains roughly planar, which is the most stable conformation. Energy fluctuations due to the bath eliminates these two distinct time scales (Figure 7 and Table 1), thus showing that the bath lessens the dependence of the isomerization process on initial conditions.

**3.5. Nonradiative Relaxation Following High-Energy Photoexcitation.** Figure 8A shows the evolution of the adiabatic state populations for $S_1$ and $S_m$ following photoexcitation to the initial high-energy state $S_m$, where *m* corresponds to the range of states that is an average of 4.5 eV above $S_0$. Following high-energy photoexcitation, the molecule relaxes nonadiabatically to $S_1$. The initial $S_m$ state persists for about 100 to 150 fs in $\epsilon = 1$ and ethanol, respectively, after which $S_1$ is primarily populated for the remainder of the 1 ps dynamics. The molecule remains *t*-SQ throughout the 1 ps nonadiabatic dynamics (inset of Figure 8A), which demonstrates that isomerization is roughly independent of photoexcitation energy; relaxation back to $S_1$ occurs on an ultrafast time scale (i.e., on the order of 100 fs) whereas isomerization occurs on a much longer time scale (Table 1).

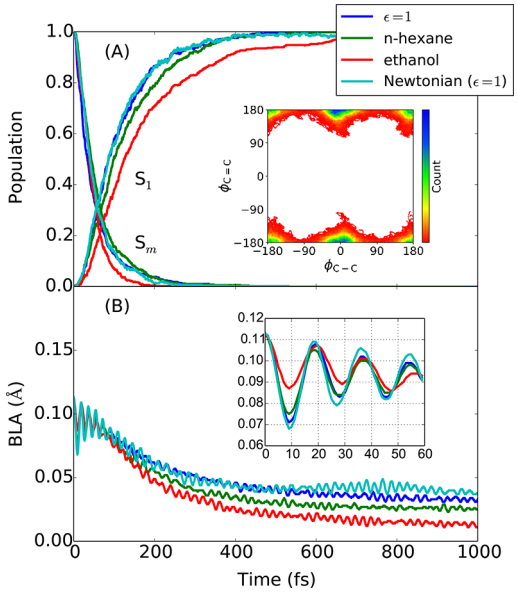


**Figure 8.** (A) Excited state populations as a function of time. The populations labeled by $S_m$ are the initial excitations—the combination of all high-lying excited states with nonzero population at time $t = 0$ fs. (B) The bond length alternation (BLA) of adjacent carbon–carbon atoms connecting the quinoline and benzene ring systems. BLA is defined as $[(b_1 + b_3)/2 - b_2]$, where $b_1$ and $b_3$ are C–C bonds and $b_2$ is the C=C bond. The inset shows coherent oscillations of the BLA within the first 60 fs.

Vibrational dynamics due to the high-energy photoexcitation is apparent from the bond length alternation (BLA) between the adjacent carbon–carbon atoms connecting the quinoline and phenyl rings reflecting C–C and C=C stretching motions.[48] The evolution of the average value of BLA is depicted in Figure 8B. Coherent oscillations, with relatively large amplitude, occur in the first 60 fs (inset of Figure 8B). These coherent vibronic dynamics are a result of the


DOI: 10.1021/acs.jpca.8b09103
J. Phys. Chem. A 2018, 122, 9403–9411

nonadiabatic transitions between excited states that are associated with molecular wave functions with varying number of nodes.[61] The amplitude of the oscillations in Figure 8B subsequently decreases in time as *t*-SQ occupies lower-lying excited states. Besides a dampening of the coherent oscillations, BLA decreases in time because the molecular wave function is more delocalized in lower-lying states and has fewer nodes. Small values of BLA are generally associated with more effective $\pi$-conjugation and corresponds to increased exciton delocalization. BLA further decreases in more polar solvents due to solvent-stable resonance structures, indicative of the increased conjugation; *t*-SQ becomes polarized since nitrogen is electron withdrawing and as a result, bond orders of the adjacent carbon−carbon atoms may change from single-like to double-like in character and vice versa. Finally, further validation of NEXMD is evidenced by calculating a mass-weighted velocity autocorrelation function for each nonadiabatic simulation (Supporting Information, Figure S8); spectral peaks are broadened for simulations carried out in a constant temperature thermostat as opposed to vacuum.

## 4. SUMMARY AND CONCLUSIONS

We used the Nonadiabatic EXcited state Molecular Dynamics (NEXMD) software to study the photoisomerization of a conjugated molecule, 4-styrylquinoline (SQ), in different environments and with different initial conditions. The study confirms that NEXMD simulations are capable of reproducing experimental observations for the complex photoisomerization process involving conical intersections with the ground state. NEXMD[48,62,63] is a computationally efficient theoretical framework that enables modeling the nonadiabatic dynamics on realistic length and time scales (hundreds of atoms and tens of picoseconds). For example, we showed that NEXMD is able to recover an energy profile (Figure 5) that shows two different reaction pathways to the final stable product DHBP (Figure 1), involving a single photon or a sequential absorption of two photons. Indeed, ref27. has reported the possibility of a one photon reaction from *t*-SQ to DHBP. This result, in conjunction with agreement in absorption properties (Figure 2 and Supporting Information), validates the software's predictive capability for our reference molecule, SQ.

We investigated the effect of external stimuli (or tunable parameters) on the photoisomerization of SQ. Specifically, solvation, photoexcitation energy, and thermostat were considered. Using an implicit linear response solvent model (i.e., the conductor-like polarizable continuum model), we found that isomerization (specifically, *t*-SQ → *p*-SQ) is twice as fast in ethanol than it is in *n*-hexane (Figure 7A), which is a consequence of further stabilization of $S_1$ relative to $S_0$ (ca. 0.25 eV). In the case of varying photoexcitation energy, dynamics beginning on $S_1$ versus a higher-lying excited state $S_m$ (due to a 4.5 eV laser excitation) did not significantly affect isomerization since relaxation to $S_1$ is on the order of 100 fs whereas isomerization, which occurs on $S_1$, is on the order of tens of ps (Table 1). The dynamics in vacuum shows that trajectories approach the conical intersection of *p*-SQ using two distinct pathways with fast and slow time scales (Figure 7B). Our analysis of the geometries from these two subsets shows that rotation of the phenyl ring destabilizes the molecule, leading to a faster transformation from *t*-SQ to *p*-SQ through rotation of $\phi_{C=C}$. Our results show that the thermostat modulates the dynamics in such a way that minimizes the dependence on initial conditions.

Future work will extend NEXMD's capabilities for modeling complex molecular processes. For example, the solvation model of this work assumes that solute and solvent polarizations are equilibrated with one another. A natural extension of this work would be to determine how non-equilibrium[64] or state-specific[50,65] solvation affects photoisomerization. Furthermore, since polarization is one of the many interactions that can take place, explicit solvation is likely important for more chemical insight. There is an ongoing effort to implement a QM/MM solvent model to NEXMD. Other work of interest would be modeling the coherent control of quantum dynamics with laser pulses.

## ■ ASSOCIATED CONTENT

### Supporting Information

The Supporting Information is available free of charge on the ACS Publications website at DOI: 10.1021/acs.jpca.8b09103.

Comparison between DFT and semiempirical levels of theory, potential energy surface (PES) scan, molecular orbitals (MOs) of SQ conformations during isomerization, time-domain isomerization data from experiment, NEXMD simulations in vacuum, and vibrational spectra during nonadiabatic dynamics (PDF)

## ■ AUTHOR INFORMATION


### Corresponding Author

*(S.T.) E-mail: serg@lanl.gov.

### ORCID

Andrew E. Sifain: 0000-0002-2964-1923
Brendan J. Gifford: 0000-0002-4116-711X
Tammie R. Nelson: 0000-0002-3173-5291
Sergei Tretiak: 0000-0001-5547-3647


### Notes

The authors declare no competing financial interest.

## ■ ACKNOWLEDGMENTS

The authors acknowledge support of the U.S. Department of Energy through the Los Alamos National Laboratory (LANL) LDRD Program. LANL is operated by Los Alamos National Security, LLC, for the National Nuclear Security Administration of the U.S. Department of Energy under Contract DE-AC52- 06NA25396. This work was done in part at the Center for Nonlinear Studies (CNLS) and the Center for Integrated Nanotechnologies (CINT) at LANL. We also acknowledge the LANL Institutional Computing (IC) program for providing computational resources. A.E.S. acknowledges support of the US Department of Energy, Grant No. DE-SC0014429. A.E.S. thanks CNLS for their support and hospitality.

## ■ REFERENCES


(1) Levine, B. G.; Martínez, T. J. Isomerization through Conical Intersections. *Annu. Rev. Phys. Chem.* **2007**, *58*, 613−634.

(2) Dugave, C.; Demange, L. Cis−Trans Isomerization of Organic Molecules and Biomolecules: Implications and Applications. *Chem. Rev.* **2003**, *103*, 2475−2532.

(3) González, L.; Escudero, D.; Serrano-Andrés, L. Progress and Challenges in the Calculation of Electronic Excited States. *ChemPhysChem* **2012**, *13*, 28−51.

(4) Polli, D.; Altoè, P.; Weingart, O.; Spillane, K. M.; Manzoni, C.; Brida, D.; Tomasello, G.; Orlandi, G.; Kukura, P.; Mathies, R. A.; et al. Conical Intersection Dynamics of the Primary Photoisomerization Event in Vision. *Nature* **2010**, *467*, 440−443.




DOI: 10.1021/acs.jpca.8b09103
J. Phys. Chem. A 2018, 122, 9403−9411

(5) Mammana, A.; Carroll, G. T.; Areephong, J.; Feringa, B. L. A Chiroptical Photoswitchable DNA Complex. *J. Phys. Chem. B* **2011**, *115*, 11581−11587.
(6) Kandori, H. Ion-Pumping Microbial Rhodopsins. *Front. Mol. Biosci.* **2015**, *2*, 52.
(7) Tanaka, K.; Toda, F. Solvent-Free Organic Synthesis. *Chem. Rev.* **2000**, *100*, 1025−1074.
(8) Briand, J.; Bräm, O.; Réhault, J.; Léonard, J.; Cannizzo, A.; Chergui, M.; Zanirato, V.; Olivucci, M.; Helbing, J.; Haacke, S. Coherent Ultrafast Torsional Motion and Isomerization of a Biomimetic Dipolar Photoswitch. *Phys. Chem. Chem. Phys.* **2010**, *12*, 3178−3187.
(9) Ercole, F.; Davis, T. P.; Evans, R. A. Photo-Responsive Systems and Biomaterials: Photochromic Polymers, Light-Triggered Self-Assembly, Surface Modification, Fluorescence Modulation and Beyond. *Polym. Chem.* **2010**, *1*, 37−54.
(10) Huang, K.; Wan, M. Self-Assembled Polyaniline Nanostructures with Photoisomerization Function. *Chem. Mater.* **2002**, *14*, 3486−3492.
(11) Kawata, S.; Kawata, Y. Three-Dimensional Optical Data Storage using Photochromic Materials. *Chem. Rev.* **2000**, *100*, 1777−1788.
(12) Irie, M.; Fukaminato, T.; Sasaki, T.; Tamai, N.; Kawai, T. Organic Chemistry: A Digital Fluorescent Molecular Photoswitch. *Nature* **2002**, *420*, 759−760.
(13) Corredor, C. C.; Huang, Z.-L.; Belfield, K. D. Two-Photon 3D Optical Data Storage via Fluorescence Modulation of an Efficient Fluorene Dye by a Photochromic Diarylethene. *Adv. Mater.* **2006**, *18*, 2910−2914.
(14) Martínez, T. J. Insights for Light-Driven Molecular Devices from Ab Initio Multiple Spawning Excited-State Dynamics of Organic and Biological Chromophores. *Acc. Chem. Res.* **2006**, *39*, 119−126.
(15) Velsko, S. P.; Fleming, G. R. Photochemical Isomerization in Solution. Photophysics of Diphenyl Butadiene. *J. Chem. Phys.* **1982**, *76*, 3553−3562.
(16) Rothenberger, G.; Negus, D.; Hochstrasser, R. Solvent Influence on Photoisomerization Dynamics. *J. Chem. Phys.* **1983**, *79*, 5360−5367.
(17) Hicks, J.; Vandersall, M.; Babarogic, Z.; Eisenthal, K. B. The Dynamics of Barrier Crossings in Solution: The Effect of a Solvent Polarity-Dependent Barrier. *Chem. Phys. Lett.* **1985**, *116*, 18−24.
(18) Barbara, P. F.; Jarzeba, W. Dynamic Solvent Effects on Polar and Nonpolar Isomerizations. *Acc. Chem. Res.* **1988**, *21*, 195−199.
(19) Pappalardo, R. R.; Sanchez Marcos, E.; Ruiz-Lopez, M. F.; Rinaldi, D.; Rivail, J. L. Solvent Effects on Molecular Geometries and Isomerization Processes: A Study of Push-Pull Ethylenes in Solution. *J. Am. Chem. Soc.* **1993**, *115*, 3722−3730.
(20) Chang, C.-W.; Lu, Y.-C.; Wang, T.-T.; Diau, E. W.-G. Photoisomerization Dynamics of Azobenzene in Solution with S1 Excitation: A Femtosecond Fluorescence Anisotropy Study. *J. Am. Chem. Soc.* **2004**, *126*, 10109−10118.
(21) Ding, J.; Desikan, V.; Han, X.; Xiao, T. L.; Ding, R.; Jenks, W. S.; Armstrong, D. W. Use of Chiral Ionic Liquids as Solvents for the Enantioselective Photoisomerization of Dibenzobicyclo [2.2. 2] Octatrienes. *Org. Lett.* **2005**, *7*, 335−337.
(22) Dokic, J.; Gothe, M.; Wirth, J.; Peters, M. V.; Schwarz, J.; Hecht, S.; Saalfrank, P. Quantum Chemical Investigation of Thermal Cis-to-Trans Isomerization of Azobenzene Derivatives: Substituent Effects, Solvent Effects, and Comparison to Experimental Data. *J. Phys. Chem. A* **2009**, *113*, 6763−6773.
(23) Mai, S.; Marquetand, P.; González, L. Intersystem Crossing Pathways in the Noncanonical Nucleobase 2-thiouracil: A Time-Dependent Picture. *J. Phys. Chem. Lett.* **2016**, *7*, 1978−1983.
(24) Talotta, F.; Heully, J.-L.; Alary, F.; Dixon, I. M.; González, L.; Boggio-Pasqua, M. Linkage Photoisomerization Mechanism in a Photochromic Ruthenium Nitrosyl Complex: New Insights from an MS-CASPT2 Study. *J. Chem. Theory Comput.* **2017**, *13*, 6120−6130.
(25) Bao, J.; Weber, P. M. Electronic Effects on Photochemistry: The Diverse Reaction Dynamics of Highly Excited Stilbenes and Azobenzene. *J. Am. Chem. Soc.* **2011**, *133*, 4164−4167.
(26) Aramendia, P. F.; Negri, R. M.; Roman, E. S. Temperature Dependence of Fluorescence and Photoisomerization in Symmetric Carbocyanines. Influence of Medium Viscosity and Molecular Structure. *J. Phys. Chem.* **1994**, *98*, 3165−3173.
(27) Budyka, M. F.; Potashova, N. I.; Gavrishova, T. N.; Lee, V. M. Solvent-Driven Adiabatic Trans-to-Cis Photoisomerization of 4-styrylquinoline. *J. Photochem. Photobiol., A* **2009**, *203*, 100−104.
(28) Schultz, T.; Quenneville, J.; Levine, B.; Toniolo, A.; Martínez, T. J.; Lochbrunner, S.; Schmitt, M.; Shaffer, J. P.; Zgierski, M. Z.; Stolow, A. Mechanism and Dynamics of Azobenzene Photoisomerization. *J. Am. Chem. Soc.* **2003**, *125*, 8098−8099.
(29) Cembran, A.; Bernardi, F.; Garavelli, M.; Gagliardi, L.; Orlandi, G. On the Mechanism of the Cis−Trans Isomerization in the Lowest Electronic States of Azobenzene: $S_0$, $S_1$, and $T_1$. *J. Am. Chem. Soc.* **2004**, *126*, 3234−3243.
(30) Weingart, O.; Lan, Z.; Koslowski, A.; Thiel, W. Chiral Pathways and Periodic Decay in Cis-Azobenzene Photodynamics. *J. Phys. Chem. Lett.* **2011**, *2*, 1506−1509.
(31) Bandara, H. D.; Burdette, S. C. Photoisomerization in Different Classes of Azobenzene. *Chem. Soc. Rev.* **2012**, *41*, 1809−1825.
(32) Neukirch, A. J.; Shamberger, L. C.; Abad, E.; Haycock, B. J.; Wang, H.; Ortega, J.; Prezhdo, O. V.; Lewis, J. P. Nonadiabatic Ensemble Simulations of Cis-Stilbene and Cis-Azobenzene Photoisomerization. *J. Chem. Theory Comput.* **2014**, *10*, 14−23.
(33) Frederick, J. H.; Fujiwara, Y.; Penn, J. H.; Yoshihara, K.; Petek, H. Models for Stilbene Photoisomerization: Experimental and Theoretical Studies of the Excited-State Dynamics of 1, 2-Diphenylcycloalkenes. *J. Phys. Chem.* **1991**, *95*, 2845−2858.
(34) Saltiel, J.; Waller, A.; Sears, D. Dynamics of Cis-Stilbene Photoisomerization: The Adiabatic Pathway to Excited Trans-Stilbene. *J. Photochem. Photobiol., A* **1992**, *65*, 29−40.
(35) Leitner, D. M.; Levine, B.; Quenneville, J.; Martínez, T. J.; Wolynes, P. G. Quantum Energy Flow and Trans-Stilbene Photoisomerization: An Example of a Non-RRKM Reaction. *J. Phys. Chem. A* **2003**, *107*, 10706−10716.
(36) Quenneville, J.; Martinez, T. J. Ab Initio Study of Cis−Trans Photoisomerization in Stilbene and Ethylene. *J. Phys. Chem. A* **2003**, *107*, 829−837.
(37) Ben-Nun, M.; Martinez, T. J. Ab Initio Molecular Dynamics Study of Cis−Trans Photoisomerization in Ethylene. *Chem. Phys. Lett.* **1998**, *298*, 57−65.
(38) Fernandez-Alberti, S.; Kleiman, V. D.; Tretiak, S.; Roitberg, A. E. Nonadiabatic Molecular Dynamics Simulations of the Energy Transfer Between Building Blocks in a Phenylene Ethynylene Dendrimer. *J. Phys. Chem. A* **2009**, *113*, 7535−7542.
(39) Fernandez-Alberti, S.; Kleiman, V. D.; Tretiak, S.; Roitberg, A. E. Unidirectional Energy Transfer in Conjugated Molecules: The Crucial Role of High-Frequency C≡C Bonds. *J. Phys. Chem. Lett.* **2010**, *1*, 2699−2704.
(40) Fernandez-Alberti, S.; Roitberg, A. E.; Kleiman, V. D.; Nelson, T.; Tretiak, S. Shishiodoshi Unidirectional Energy Transfer Mechanism in Phenylene Ethynylene Dendrimers. *J. Chem. Phys.* **2012**, *137*, 22A526.
(41) Soler, M. A.; Roitberg, A. E.; Nelson, T.; Tretiak, S.; Fernandez-Alberti, S. Analysis of State-Specific Vibrations Coupled to the Unidirectional Energy Transfer in Conjugated Dendrimers. *J. Phys. Chem. A* **2012**, *116*, 9802−9810.
(42) Adamska, L.; Nayyar, I.; Chen, H.; Swan, A. K.; Oldani, N.; Fernandez-Alberti, S.; Golder, M. R.; Jasti, R.; Doorn, S. K.; Tretiak, S. Self-Trapping of Excitons, Violation of Condon Approximation, and Efficient Fluorescence in Conjugated Cycloparaphenylenes. *Nano Lett.* **2014**, *14*, 6539−6546.
(43) Galindo, J. F.; Atas, E.; Altan, A.; Kuroda, D. G.; Fernandez-Alberti, S.; Tretiak, S.; Roitberg, A. E.; Kleiman, V. D. Dynamics of Energy Transfer in a Conjugated Dendrimer Driven by Ultrafast


DOI: 10.1021/acs.jpca.8b09103
*J. Phys. Chem. A* 2018, 122, 9403−9411

Localization of Excitations. *J. Am. Chem. Soc.* **2015**, *137*, 11637−11644.
(44) Bricker, W. P.; Shenai, P. M.; Ghosh, A.; Liu, Z.; Enriquez, M. G. M.; Lambrev, P. H.; Tan, H.-S.; Lo, C. S.; Tretiak, S.; Fernandez-Alberti, S.; et al. Non-radiative Relaxation of Photoexcited Chlorophylls: Theoretical and Experimental Study. *Sci. Rep.* **2015**, *5*, 13625.
(45) Shenai, P. M.; Fernandez-Alberti, S.; Bricker, W. P.; Tretiak, S.; Zhao, Y. Internal Conversion and Vibrational Energy Redistribution in Chlorophyll a. *J. Phys. Chem. B* **2016**, *120*, 49−58.
(46) Alfonso Hernandez, L.; Nelson, T.; Gelin, M. F.; Lupton, J. M.; Tretiak, S.; Fernandez-Alberti, S. Interference of Interchromophoric Energy-Transfer Pathways in $\pi$-Conjugated Macrocycles. *J. Phys. Chem. Lett.* **2016**, *7*, 4936−4944.
(47) Zheng, F.; Fernandez-Alberti, S.; Tretiak, S.; Zhao, Y. Photoinduced Intra-and Intermolecular Energy Transfer in Chlorophyll a Dimer. *J. Phys. Chem. B* **2017**, *121*, 5331−5339.
(48) Sifain, A. E.; Bjorgaard, J. A.; Nelson, T. R.; Nebgen, B. T.; White, A. J.; Gifford, B. J.; Gao, D. W.; Prezhdo, O. V.; Fernandez-Alberti, S.; Roitberg, A. E.; et al. Photoexcited Nonadiabatic Dynamics of Solvated Push-Pull $\pi$-Conjugated Oligomers with the NEXMD Software. *J. Chem. Theory Comput.* **2018**, *14*, 3955−3966.
(49) Dewar, M. J.; Zoebisch, E. G.; Healy, E. F.; Stewart, J. J. Development and Use of Quantum Mechanical Molecular Models. 76. AM1: A New General Purpose Quantum Mechanical Molecular Model. *J. Am. Chem. Soc.* **1985**, *107*, 3902−3909.
(50) Bjorgaard, J. A.; Kuzmenko, V.; Velizhanin, K.; Tretiak, S. Solvent Effects in Time-Dependent Self-Consistent Field Methods. I. Optical Response Calculations. *J. Chem. Phys.* **2015**, *142*, No. 044103.
(51) Masunov, A.; Tretiak, S.; Hong, J. W.; Liu, B.; Bazan, G. C. Theoretical Study of the Effects of Solvent Environment on Photophysical Properties and Electronic Structure of Paracyclophane Chromophores. *J. Chem. Phys.* **2005**, *122*, 224505.
(52) Mukamel, S.; Tretiak, S.; Wagersreiter, T.; Chernyak, V. Electronic Coherence and Collective Optical Excitations of Conjugated Molecules. *Science* **1997**, *277*, 781−787.
(53) Tretiak, S.; Mukamel, S. Density Matrix Analysis and Simulation of Electronic Excitations in Conjugated and Aggregated Molecules. *Chem. Rev.* **2002**, *102*, 3171−3212.
(54) Ramachandran, G.; Ramakrishnan, C.; Sasisekharan, V. Stereochemistry of Polypeptide Chain Configurations. *J. Mol. Biol.* **1963**, *7*, 95−99.
(55) Levine, B. G.; Ko, C.; Quenneville, J.; MartÍnez, T. J. Conical Intersections and Double Excitations in Time-Dependent Density Functional Theory. *Mol. Phys.* **2006**, *104*, 1039−1051.
(56) Vincent, J. C.; Muuronen, M.; Pearce, K. C.; Mohanam, L. N.; Tapavicza, E.; Furche, F. That Little Extra Kick: Nonadiabatic Effects in Acetaldehyde Photodissociation. *J. Phys. Chem. Lett.* **2016**, *7*, 4185−4190.
(57) Tully, J. C. Molecular Dynamics with Electronic Transitions. *J. Chem. Phys.* **1990**, *93*, 1061−1071.
(58) Nelson, T.; Fernandez-Alberti, S.; Roitberg, A. E.; Tretiak, S. Nonadiabatic Excited-State Molecular Dynamics: Treatment of Electronic Decoherence. *J. Chem. Phys.* **2013**, *138*, 224111.
(59) Fernandez-Alberti, S.; Roitberg, A. E.; Nelson, T.; Tretiak, S. Identification of Unavoided Crossings in Nonadiabatic Photoexcited Dynamics Involving Multiple Electronic States in Polyatomic Conjugated Molecules. *J. Chem. Phys.* **2012**, *137*, No. 014512.
(60) Magyar, R.; Tretiak, S.; Gao, Y.; Wang, H.-L.; Shreve, A. A Joint Theoretical and Experimental Study of Phenylene−Acetylene Molecular Wires. *Chem. Phys. Lett.* **2005**, *401*, 149−156.
(61) Nelson, T. R.; Ondarse-Alvarez, D.; Oldani, N.; Rodriguez-Hernandez, B.; Alfonso-Hernandez, L.; Galindo, J. F.; Kleiman, V. D.; Fernandez-Alberti, S.; Roitberg, A. E.; Tretiak, S. Coherent Exciton-Vibrational Dynamics and Energy Transfer in Conjugated Organics. *Nat. Commun.* **2018**, *9*, 2316.
(62) Nelson, T.; Fernandez-Alberti, S.; Chernyak, V.; Roitberg, A. E.; Tretiak, S. Nonadiabatic Excited-State Molecular Dynamics Modeling of Photoinduced Dynamics in Conjugated Molecules. *J. Phys. Chem. B* **2011**, *115*, 5402−5414.
(63) Nelson, T.; Fernandez-Alberti, S.; Roitberg, A. E.; Tretiak, S. Nonadiabatic Excited-State Molecular Dynamics: Modeling Photophysics in Organic Conjugated Materials. *Acc. Chem. Res.* **2014**, *47*, 1155−1164.
(64) Bjorgaard, J. A.; Velizhanin, K. A.; Tretiak, S. Nonequilibrium Solvent Effects in Born-Oppenheimer Molecular Dynamics for Ground and Excited Electronic States. *J. Chem. Phys.* **2016**, *144*, 154104.
(65) Bjorgaard, J. A.; Velizhanin, K. A.; Tretiak, S. Solvent Effects in Time-Dependent Self-Consistent Field Methods. II. Variational Formulations and Analytical Gradients. *J. Chem. Phys.* **2015**, *143*, No. 054305.
(66) The $S_0/S_1$ conical intersection may not be accurately described with the NEXMD level of theory. Setting a 1.0 eV threshold on the energy gap ensures that dynamics are sufficiently far from the conical intersection. Nonadiabatic transitions are likely to occur at much smaller energy gaps, typically less than 0.1 eV.[48]


DOI: 10.1021/acs.jpca.8b09103
*J. Phys. Chem. A* 2018, 122, 9403−9411